IES Calibration and Mapping Procedures

KAREN L. TRACEY, STEPHAN D. HOWDEN, AND D. RANDOLPH WATTS

Graduate School of Oceanography, University of Rhode Island, Narragansett, Rhode Island

(Manuscript received 1 August 1996, in final form 24 January 1997)

ABSTRACT

The procedures used in the Synoptic Ocean Prediction experiment for calibration of inverted echo sounder (IES) travel time τ data have led to substantially improved accuracy. In previous work, τ was converted to main thermocline depth Z_T using point measurements of the 12°C depth from coincident expendable bathythermograph (XBT) casts. The new method presented in this study vertically integrates the XBT temperature to produce the quantity Q_T, which is very tightly related to τ. The advantage of this method is that the calibration constants have roughly half the uncertainty obtained with the traditional method. Seasonal changes in τ determined from hydrographic data in the Gulf Stream region were found to vary with geographic region; near 68°W τ changed by 1.8 ms from March to September, whereas near Cape Hatteras the annual change was only 1.0 ms. The fully calibrated IES Z_T^* has an estimated error of 19 m (one standard deviation). An iterative optimal interpolation scheme is described, by which the Gulf Stream thermocline depth was mapped on a two-dimensional grid. Initially, daily maps were generated using established mapping techniques. Subsequently, these maps were averaged for 31-day periods and in turn used as the new ''mean fields'' for the final maps. Verification of the mapped fields against independent XBT data gives rms differences of 31–46 m, which is only 3%–5% of the 900-m range of the observed Z_T^*.

1. Introduction

Inverted echo sounders (IESs) have been used to monitor oceanic fronts since the 1970s after Rossby (1969) first introduced the concept of using variations in acoustic travel time τ to measure changes in the depth of the main thermocline. IESs were initially deployed in the MODE (Mid Ocean Dynamics Experiment) region by Watts and Rossby (1977) in a study that showed linear relationships also exist between travel time and several quantities: thermocline depth Z_T, full water column dynamic height ΔD, and heat content Q_h. Since then, IESs have been used extensively in the Gulf Stream between Florida and the Grand Banks (Watts and Johns 1982; Li et al. 1985; Tracey and Watts 1986; Hallock 1992) as well as in other oceanic regions (Miller et al. 1985; Chiswell et al. 1986; Katz 1987; James et al. 1994). IESs have been deployed at individual sites for long-term monitoring (Chiswell 1994), in cross-stream lines to monitor the location of fronts (Watts and Johns 1982), or in large arrays to map the thermal structure in two-dimensional regions (Watts et al. 1989).

Calibrating the travel time measurements into other scientific quantities requires knowledge of the variations in temperature and salinity stratification and the resulting density and sound speed profiles in the region where the IES is deployed. Hydrographic data, either historical or taken repeatedly during the IES deployment period, are used to determine the slopes of the linear relationships between τ and ΔD, Z_T, or Q_h (Watts and Johns 1982; Hallock 1987; Trivers and Wimbush 1994; Chiswell 1994; James and Wimbush, 1995). To determine absolute Z_T or ΔD (not just the variability), an additive calibration constant is required for each instrument site. These constants are typically determined by taking expendable bathythermographs (XBTs for Z_T) or CTD (conductivity–temperature–depth) hydrocasts (for ΔD and Q_h) at the IES sites. The latter integral quantities have substantially better correlation (less scatter) with τ, which is also a vertical integral quantity. However, since XBTs require substantially less ship time and processing, we were motivated to find a way to make the XBT data better suited for calibration purposes.

Unlike the integral quantities ΔD and Q_h, the point measurements of thermocline depths from XBTs are sensitive to small-scale perturbations in the water column, unnecessarily increasing the uncertainty in the calibration constant. To remove these errors, a new approach was devised such that vertically integrated XBT temperatures were used in the calibration process, thereby eliminating the noisier point measurements. By integrating the temperatures between 200 m and the maximum probe depth of 750 m, the quantity Q_T was obtained for each XBT. Here, Q_T is tightly related to Q_h as well as to ΔD and τ in the Slope Water/Gulf Stream/

Corresponding author address: Dr. D. Randolph Watts, Graduate School of Oceanography, University of Rhode Island, Narragansett Bay Campus, Narragansett, RI 02882-1197.

Sargasso Sea system. These close interrelationships arise because all of the variables change systematically as the thermocline depth Z_T varies. In this paper, the empirical relationship between Q_T and Z_T is fitted by an analytic function. Thermocline depths obtained from XBTs using this relationship yield more accurate calibration constants.

Calibrated IES data from arrays of instruments have been used to produce gridded fields of the thermocline depth (Watts et al. 1989). Such maps have been used in tracking the position of the Gulf Stream front as well as the thermal structure of the adjacent eddy fields (Hallock 1992; Watts et al. 1995). Kim and Watts (1994) and He (1993) describe further applications of these maps, in which Z_T fields from the Gulf Stream are treated as proportional to the geostrophic streamfunction. Gridded fields of velocity and vorticity were obtained by differentiating the streamfunctions.

Initial attempts to repeat these analyses on data from the Synoptic Ocean Prediction (SYNOP) experiment near 68°W, where the measurement array was more widely spaced, were somewhat discouraging. Although the Z_T maps were shown to track the path of the Gulf Stream quite well, differentiating them to obtain the dynamically interesting quantities velocity and vorticity produced less than satisfactory results. Because the current vectors derived from the maps either under- or overestimated the observed speeds, the mapping procedures did not adequately resolve the lateral gradients of the thermocline depth. Our desire to determine these dynamic fields accurately led to the development of the improved mapping techniques documented in this paper. An iterative mapping scheme that produces Z_T fields with well-resolved thermal gradients is described.

As part of the SYNOP experiment, IESs were deployed together with current meter moorings and bottom pressure sensors in the Gulf Stream (Watts et al. 1995; Shay et al. 1995). Thus we could cross-check our analysis procedures by intercomparing the various datasets. Section 2 describes the data. Section 3 discusses improvements made to the IES calibration procedures using vertically integrated temperature profiles and a correction applied to the travel time measurements to reduce the effects of seasonal warming. Section 4 presents the iterative scheme used to map the thermocline topography in the SYNOP arrays. The accuracy of these maps is also discussed.

2. Description of the data

From 1988 to 1990, IESs were deployed in two arrays in the Gulf Stream (Fig. 1). Nine IESs were moored in the Inlet Array, near Cape Hatteras, and 24 IESs were located on five transects in the Central Array, centered near 68°W. The IESs were deployed with typical durations of 1 year, and altogether 65 records required calibration from travel time τ to thermocline depth Z_T.

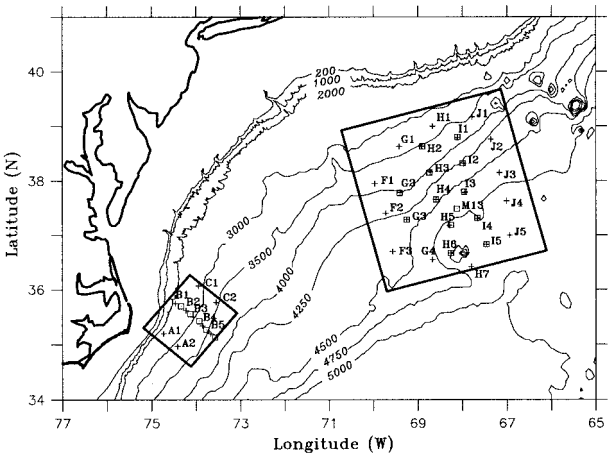

FIG. 1. The SYNOP Inlet and Central Arrays. Inverted echo sounder sites are denoted by the plus symbols and current meter moorings by the open squares. The bold boxes indicate the regions that have been mapped by optimal interpolation. Bathymetric contours are in meters.

Current meter moorings and bottom pressure sensors were also deployed at 12 sites in the Central Array.

Numerous XBTs were taken on the four cruises to deploy and recover the IESs. One cruise was aboard the R/V *Endeavor* (EN216–August 1990) and three on the R/V *Oceanus* (OC200–May 1988, OC207–June 1989, and OC210–August 1989). XBTs were taken at each IES site for calibration purposes and also at other locations to survey the Gulf Stream path in both array regions during each cruise.

XBTs were also taken in the Central Array as part of another program—the Anatomy of Gulf Stream Meanders experiment (Hummon et al. 1991). This experiment conducted two cruises aboard the R/V *Endeavor* (EN185–September 1988 and EN194–April 1989) to survey the dynamic structure and evolution of Gulf Stream meanders. Fortuitously, portions of their surveys overlapped the Central Array.

The IES Z_T data were mapped onto gridded fields using the optimal interpolation method described in section 4. Additionally, Z_T data obtained from temperature measurements on the current meter moorings also were incorporated into these maps at sites where IES data were lacking. Cronin (1993) discusses the technique used to obtain thermocline depth estimates from the moored temperature data. Specifically, during the May 1988–May 1989 period, two moored temperature records (sites H2 and I3) were used for the full time period, and the temperatures at site I1 for a 4-month period. Moored temperature data from sites M13 and I1 were used during the August 1989–August 1990 period. The inclusion of these data improved the maps primarily by sharpening the lateral gradients of the thermocline in regions where otherwise there would have been data gaps. The Z_T measurements obtained from the XBTs of all six cruises were used to evaluate these thermocline depth maps. The moored current meter data will also

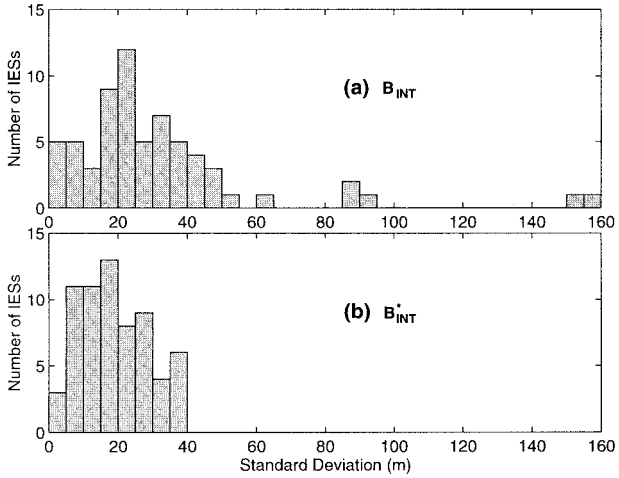

FIG. 2. Distribution of the (a) B_{INT} and (b) B^*_{INT} standard deviations obtained for 65 SYNOP IESs.

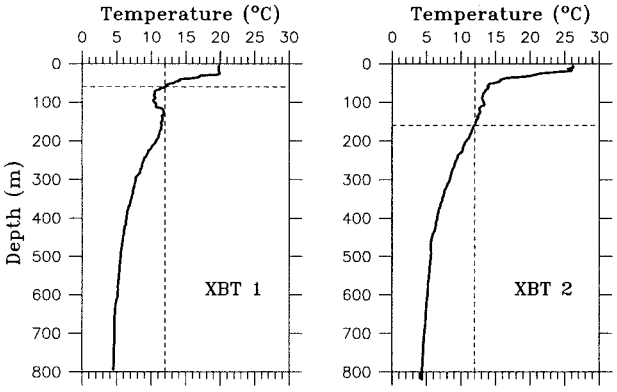

FIG. 3. Temperature profiles of two XBTs used to calibrate an IES. The dashed lines highlight the 12°C isotherm depth.

be used directly in section 4 to check the accuracy with which the Z_T fields may be differentiated to yield geostrophic velocities.

3. IES processing updates

a. Calibration into thermocline depth

Rossby (1969) showed that IES travel time measurement τ is linearly proportional to the depth of the main thermocline Z_T, such that

$$Z_T = A\tau + B_{\text{INT}}. \tag{1}$$

The slope A depends on the local T–S properties and is uniform for large geographic regions. For the Gulf Stream region extending eastward from Cape Hatteras to 65°W, the slope is -20.256 m ms^{-1}. The calibration constant B_{INT} must be determined for each IES site because it depends on the depth at which the instrument is moored.

To determine the calibration constant B_{INT}, the depth of the thermocline at the instrument site must be measured while the IES is sampling. In previous studies (Fuglister and Voorhis 1965; Watts and Johns 1982), the Gulf Stream thermal front has been represented by the depth of an individual isotherm. The 12°C isotherm was chosen for our Gulf Stream work ($Z_T = Z_{12}$). One common method of obtaining Z_{12} is to use the temperature profiles of the XBTs since they are relatively inexpensive and convenient to use.

After Z_{12} has been determined from each XBT, the IES calibration is accomplished by choosing the τ measurements that are most nearly coincident in time with the launch of the XBT probes. (Since the SYNOP IESs were usually sampled every half hour, the time offset rarely exceeded 15 min.) Since the slope A is known, B_{INT} can be calculated for each (Z_{12}, τ) pair using Eq. (1). Typically, two to six XBTs were dropped at each site throughout the deployment period, and the best estimate of the true calibration constant was obtained by averaging the individual estimates.

$$B_{\text{INT}} = \frac{1}{N}\sum_{j=1}^{N}(Z_{12} - A\tau), \tag{2}$$

where N is the number of XBTs dropped at the IES site.

The standard deviation σ_{12} of B_{INT} gives the accuracy of the calibration from travel time into Z_{12}. For all SYNOP IESs, σ_{12} were calculated, and a distribution plot of their values is shown in Fig. 2a. Half of the σ_{12} range between 10 and 30 m, which is an acceptable level of accuracy given the total thermocline depth variation of 900 m. However, several σ_{12} values exceed 60 m, which motivated us to seek an improved calibration method.

The two XBT profiles in Fig. 3 illustrate how these larger σ_{12} arise. In this example, the τ measured by the IES at the drop times of XBTs 1 and 2 were 252.4l and 252.17 ms, respectively. The difference is only 0.24 ms, which would correspond to approximately a 5-m change in the thermocline depth. However, the actual Z_{12} values of 60 and 159 m measured by the two XBTs differ by nearly 100 m, and the corresponding B_{INT} (5173.2 m for XBT 1 and 5267.8 m for XBT 2) differ by almost as much. Within the main thermocline region the vertical distances between isotherms can be compressed or expanded by processes of small vertical scale, such as intrusions or internal waves. Individual isotherms may be displaced without a corresponding change in the depth of the thermocline as a whole. For the two XBTs shown in Fig. 3, if a different isotherm (e.g., 11°C) had been chosen to represent the thermocline, very similar depths would have been obtained. Any single isotherm depth, being a point measurement, is sensitive to these small-scale perturbations, which can lead to outliers and large variation in the calibration constants.

A quantity that would better characterize the depth of the main thermocline would vary only with the thermocline as a whole. The method described here takes advantage of a finding by Watts and Rossby (1977) that the heat content of a column of water Q_h is also linearly

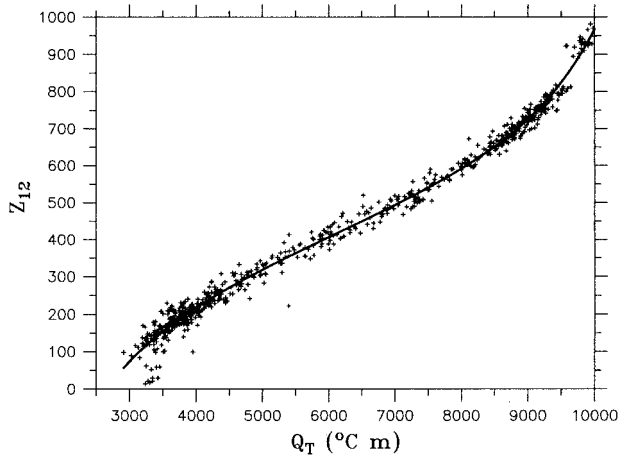

FIG. 4. The point measurement of 12°C depth, Z_{12} (no asterisk) vs $Q_T = \int_{200}^{750} T\,dz$ from the SYNOP XBT casts. Superimposed is the best-fit curve Z_{12}^* (Q_T) (including asterisk) defined in Eq. (3).

related to the depth of the main thermocline. The vertically integrated temperature Q_h is a good measure of Q_h because the heat capacity of sea water is essentially independent of salinity. For this application, XBT temperature profiles were integrated between 200 and 750 m to estimate Q_T. The upper limit of 200 m was chosen in order to remove the effects of the seasonal warming and cooling of the surface layer. The lower limit was determined by the maximum depth range of the XBT probes.

Figure 4 shows that a well-defined relationship exists between Q_T and thermocline depth, in which most of the scatter is attributed to the point measurements of Z_{12}. Superimposed on Fig. 4 is the best-fit curve to the data, which serves to filter out the scatter of the point measurements and is defined as

$$Z_{12}^* = A_1 \exp[(Q_T - Q_1)/\lambda_1] + A_2 \exp[(Q_2 - Q_T)/\lambda_2] + aQ_T + b, \quad (3)$$

where $Q_T = \int_{750\ \mathrm{m}}^{200\ \mathrm{m}} T\,dz$, $Q_1 = 9998$°C m, $Q_2 = 2912$°C m, $A_1 = 246.8$ m, $A_2 = -107.2$ m, $\lambda_1 = 918.5$°C^{-1} m^{-1}, $\lambda_2 = 904.5$°C^{-1} m^{-1}, $a = 0.0788$°C^{-1}, and $b = -65.93$ m. For each XBT, the quantity Q_T can be integrated from the temperature profile and converted into a representative thermocline depth Z_{12}^* using Eq. (3). The relationship between Q_T and Z_{12} is not linear since the temperature integration is performed over a restricted depth range (in which Z_{12} may even fall outside the range 200–750 m) instead of the entire water column. However, a functional relationship does exist such that each Q_T defines a unique Z_{12}^*.

Figure 2b illustrates the improvements to the calibrations when Q_T is used to determine the thermocline depths, as designated by asterisks on all quantities. The histogram of the σ_{12}^* of B_{INT}^* for the same SYNOP IESs is shown. The σ_{12}^* of nearly all the IESs range between 5 and 30 m, and no occurrences exceed 40 m. For the pair of XBTs in Fig. 3 discussed above, for which point measurements from the two XBTs yielded thermocline depths that differed by nearly 100 m, the Z_{12}^* values (156 m for XBT 1 and 165 m for XBT 2) differ by only 9 m. As a result, the corresponding B_{INT}^* of 5262.7 and 5268.7 m are also in good agreement. With the large outliers gone, confidence in the calibration of travel time to thermocline depth Z_{12}^* is greatly enhanced. Overall, the best estimated one standard deviation error of B_{INT}^* over all the IES sites is 19 m.

b. Seasonal correction

Simple application of Eq. (1) to the IES travel time measurements assumes that all changes in τ are caused solely by changes in the depth of the permanent thermocline. However, Rossby (1969) and Tracey and Watts (1986) note that changes in τ also occur in response to the seasonal warming and cooling of the surface layers (<200 m). Although they find that uncorrected travel times result in thermocline depth errors that are typically less than 40 m, it is nevertheless desirable to remove the seasonal variability from the τ measurements prior to calculating Z_{12}^*. The seasonal correction curve shown in Tracey and Watts (1986) was based on data from only 15 Gulf Stream cross sections presented in Iselin (1940). The following discussion describes new seasonal correction curves determined from over 30 000 XBTs in the Gulf Stream region. These seasonal correction curves have been applied to the SYNOP IES τ measurements.

To determine the seasonal variability of travel time in the surface waters, XBTs for the Gulf Stream region between Cape Hatteras and 65°W were obtained from the NODC and NavOceanO archives. The travel time in the upper 200 m (τ_{200}) was determined by integrating each XBT temperature profile assuming a standard T–S relationship. (The effect of taking a constant $S = 35$ psu would add insignificant error to this calculation.) The XBTs were grouped into several subsets to check for both cross-stream and downstream variations in the seasonal signal.

First, the XBTs were grouped according to their relative cross-stream positions. XBTs were categorized as being on either the Slope Water side ($Z_{12} < 200$ m), within the Gulf Stream ($200 \le Z_{12} \le 600$ m), or on the Sargasso Sea side ($Z_{12} > 600$ m). Monthly averages of τ_{200} were calculated for each group separately. No significant differences in the seasonal cycle were found between the three groups. The peak-to-peak range of τ_{200} was about 1.8 ms, with the longest travel times obtained during February–April and the shortest values obtained during August–October.

Subsequently, the XBTs were divided into three subsets based on geographic location, as indicated in Fig. 5. The τ_{200} data then were grouped by month and averaged. The resulting curves, which were smoothed with a 3-month low-pass filter, are also shown in the figure.

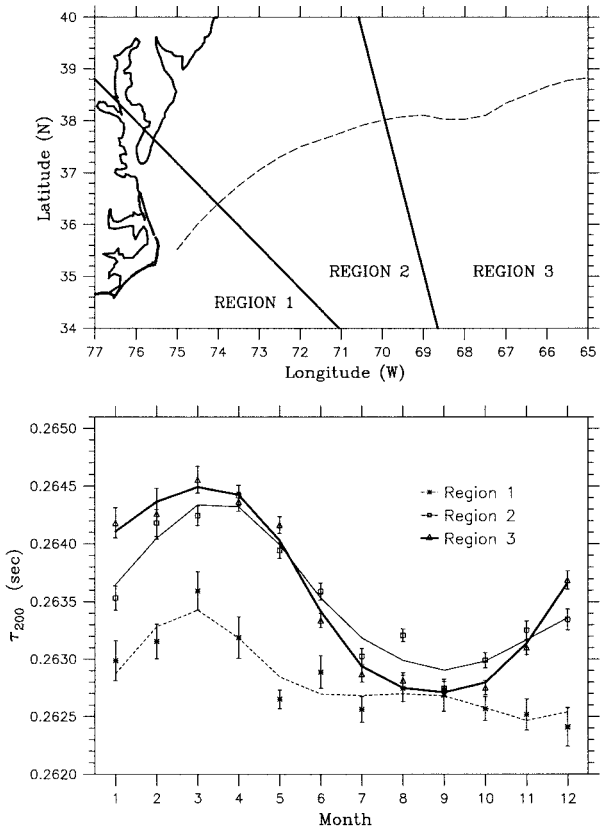

FIG. 5. (top) Bold lines delineate the three downstream regions used to categorize the XBTs. The dashed line indicates the mean location of the surface Gulf Stream thermal front during 1982–89 supplied by Lee (1994). (bottom) Monthly τ_{200} averages and standard error of the mean (with each XBT treated as independent) obtained for the three geographic regions. Curves represent 3-month low-pass filtering. Ticks on the *x* axis indicate the middle of each month.

The annual signal differs significantly between the three downstream regions. The largest seasonal change in travel time was observed in region 3 near 68°W; τ_{200} was found to vary by 1.8 ms with the maximum occurring in March and the minimum in September. (Incidentally, a 1-ms change in τ corresponds to a heat content change of 1.3×10^9 J m^{-2} in the water column. The corresponding average rate of change from March to September is about 80 W m^{-2}.) The seasonal change in τ_{200} for region 1, with a peak-to-peak range of 1.0 ms, is roughly half that of region 3. Additionally, the shape of the curve for region 1 is different; the curve is less sinusoidal with τ_{200} being nearly uniform from June to September and decreasing only slightly between October and December. The seasonal curve for region 2 is most similar to that of region 3, but the total change in τ_{200} is only 1.4 ms.

To remove the seasonal variability arising from the upper 200 m from IES τ measurements, the relative differences $\Delta\tau_{200}$ between the monthly averages and the March value were determined for each of the three curves. Then $\Delta\tau_{200}$ values were subtracted from the measured travel times. The $\Delta\tau_{200}$ values for region 1 were used to adjust the IESs from the SYNOP Inlet Array, and those for region 3 were used for the instruments in the Central Array. These $\Delta\tau_{200}$ curves represent the average seasonal progression of travel time within the upper 200 m, and we estimate that the actual seasonal signal for a particular deployment period should differ by less than 0.3 ms.

4. Objective mapping updates

Once the IES have been calibrated, the Z_{12}^* data can be used to produce mapped fields of thermocline depth within the study regions. The Z_{12}^* measurements from the SYNOP Inlet and Central Arrays, at spacings of 25–60 km, were interpolated onto 20-km, regularly spaced grids using the optimal interpolation (OI) technique described in Watts et al. (1989). Their method involves preconditioning the data prior to performing the OI in order to satisfy (in the Gulf Stream) the requirement for homogeneity; first, the mean field (alternatively called the first-guess field) is removed and then the demeaned data are normalized by the standard deviation field. The resulting perturbation data are interpolated using the Gauss–Markov method (Bretherton et al. 1976), and the mean and standard deviation fields are restored afterward to yield maps of the Z_{12}^* fields. An example of a mapped Z_{12}^* field for a single day is shown in the upper-right panel of Fig. 6; a Gulf Stream crest is in the Central Array on 3 July 1990 and a warm core ring is apparent in the upper right corner. Comparison with satellite imagery confirms that the positions of both features have been resolved by the mapping procedure. Using this method, a set of Z_{12}^* maps was generated at daily intervals for the 26-month-long SYNOP experiment.

However, inadequacies in these maps were revealed when they were subsequently differentiated to produce fields of velocity and vorticity. Using the methods described in He (1993), the Z_{12}^* maps were converted to fields of geostrophic streamfunction in order to produce gridded fields of geostrophic baroclinic velocity ($\mathbf{V}_{\mathrm{PRE}}$). The second panel of Fig. 7 shows a 2-yr time series of these derived velocities at a single site (I4) in the Central Array. The vectors indicate the baroclinic velocity between 400 and 1000 m. The top panel in Fig. 7 shows the observed shear velocities $\mathbf{V}_{\mathrm{CM}}$ determined by differencing the currents measured at 400 and 1000 m at the same location. The overall impression is that $\mathbf{V}_{\mathrm{PRE}}$ vectors provide a reasonably good representation of the observed currents, except that the speeds appear to be underestimated. Indeed the difference vectors (third panel) confirm that the speeds are biased low, but there are also occasional periods when they are overestimated. These differences indicate that the thermocline gradients were not resolved well enough in the mapped fields.

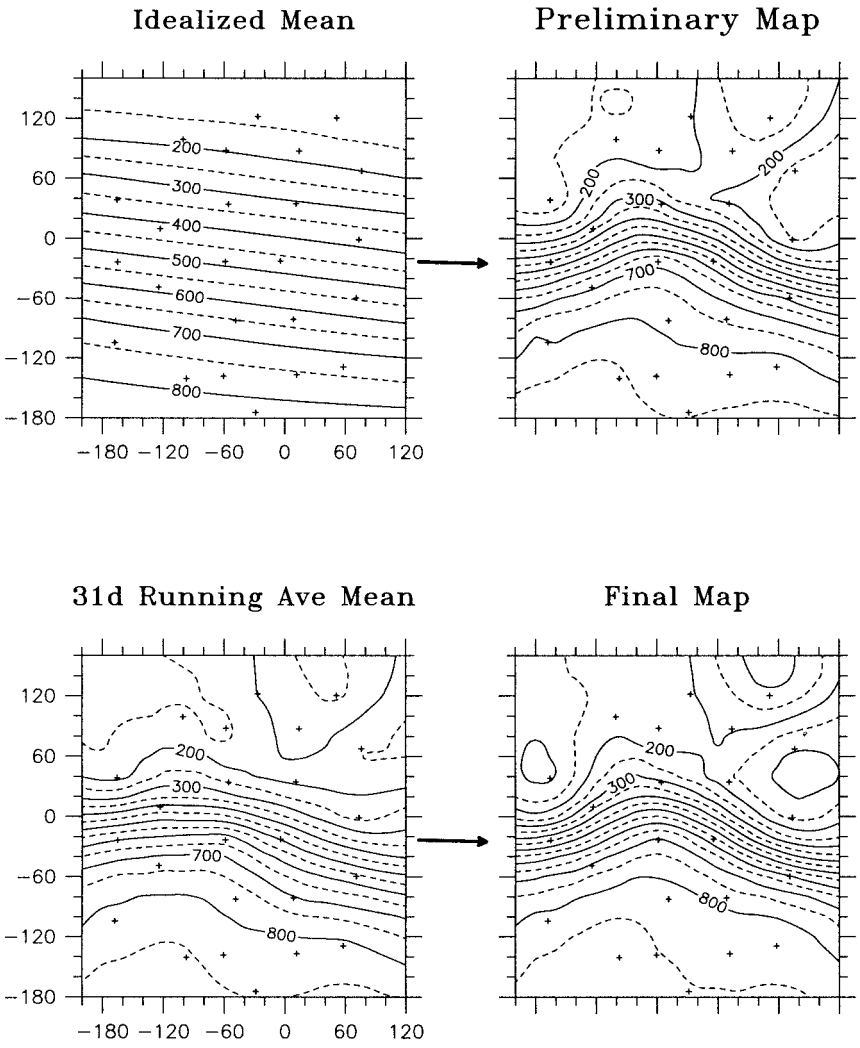

FIG. 6. Iterative optimal interpolation scheme. All frames correspond to the large boxed region in Fig. 1. The distances (in kilometers) on both axes are referenced to the grid origin at 38°N, 68°W and the x axis is oriented along 075° true. The depth of the 12°C isotherm is contoured at 50-m intervals and plus marks indicate IES sites. The idealized mean field (upper left) was used to produce the preliminary Z^*_{12} map (upper right). Subsequently, 31 daily preliminary maps were averaged to produce the field shown at the bottom left, which in turn was used as a first-guess field for optimal interpolation to produce the final Z^*_{12} map (bottom right).

a. Iterative mapping

Therefore, efforts were undertaken to improve the maps of Z^*_{12}. The new procedure employs the OI technique in an iterative fashion. The above set of Z^*_{12} maps, produced with the input data preconditioned by removing an idealized first-guess field representative of the long-term mean, was subsequently averaged, using 31-day running averages, to serve as the first-guess fields for the final set of maps.

It is important to note that a different correlation function ρ was used for this second mapping step. The correlation function ρ_{Central}, based on observed correlations and shown in Tracey and Watts (1991), was used to produce the preliminary maps. That function had long correlation length scales, with ρ falling to e^{-1} at 106 km and $\rho = 0$ at 150 km. For the second set of maps, a correlation function with shorter length scales was appropriate to fit the perturbations from the 31-day running mean fields. This second function ρ_{31} was determined by first calculating and removing the 31-day running averages from all IES measurements collected between 1979 and 1990, and then calculating their spatial correlations. An analytic function was fitted to the observed correlations:

$$\rho_{31} = F_o \exp\left[-\left(\frac{r}{a_1}\right)^2\right] \cos\left(\frac{\pi r}{2b_1}\right), \tag{4}$$

where $a_1 = 117$ km, $b_1 = 92$ km, and $\tau = [(x_i - x_j)^2$

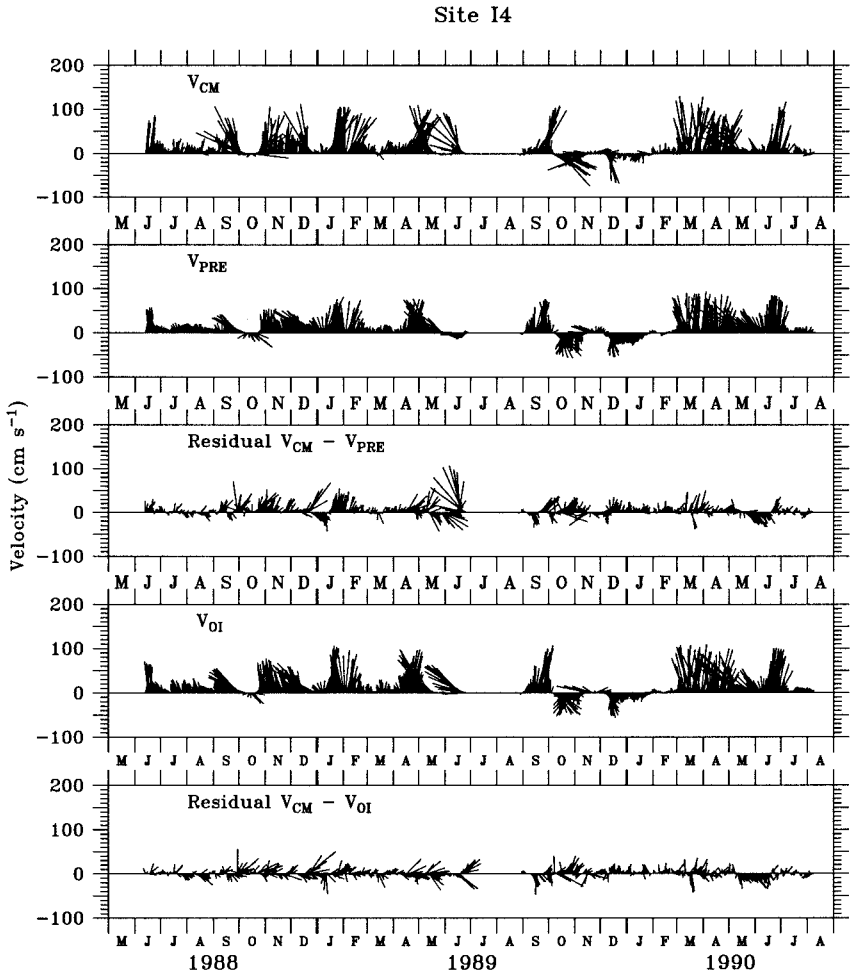

FIG. 7. (top panel) Shear velocity between 400 and 1000 m ($\boldsymbol{V}_{CM}$) measured by current meters at site 14 for the period June 1988 through August 1990. (second panel) Geostrophic velocity $\boldsymbol{V}_{PRE}$ determined at the same site from the preliminary set of IES OI maps. (third panel) The difference vectors $\boldsymbol{V}_{CM} - \boldsymbol{V}_{PRE}$. (fourth panel) Geostrophic velocity $\boldsymbol{V}_{OI}$ determined from the final set of IES OI maps. (bottom) The difference $\boldsymbol{V}_{CM} - \boldsymbol{V}_{OI}$. All vectors are plotted with eastward velocity up the page.

$+ (y_i - y_j)^2]^{1/2}$ is the distance between sites i and j. The scale factor $F_o = [(1 - \epsilon_i)(1 - \epsilon_j)]^{1/2}$, where ϵ_i and ϵ_j are the noise variance of the data. The value of ϵ was set to 0.04 for the IES measurements and 0.08 for Z^*_{12} estimates obtained from current meter temperature data. For this function, ρ_{31} decreases to e^{-1} at 65 km and crosses zero at 92 km.

The selection of 31 days as the averaging period for the mean fields was made after considerable testing. Evaluations were conducted on maps produced with averaging periods that ranged from 1 day to roughly 1 yr [for each averaging period the appropriate a_1 and b_1 were used in Eq. (4)]. For the 1-day averaging period, the previous day's map was used as the first-guess field for the current day. For maps generated with first-guess fields of 15 days or less, the length scales of the associated correlation functions were so small as to render data from adjacent IES sites uncorrelated. This was undesirable because at the second step of the iterative method, the mapped fields were updated primarily by submesoscale ''noise'' at scales smaller than the measurement grid (roughly 60 km), and the estimated error fields became unacceptably large. On the other hand, although the correlation length scales associated with perturbations from running average maps of averaging periods greater than 45 days were long enough to update the maps with true mesoscale signals, the corresponding first-guess fields were considerably broadened and smoothed by the longer averaging periods. As a result, the cross-stream gradients in those maps were resolved inadequately. Therefore, 31 days was selected for the averaging period since it satisfied the combined criteria of reducing the estimated mapping errors and retaining sharp frontal gradients, as judged by comparisons (shown next) with current meter measurements.

Figure 6 also illustrates the iterative scheme for 3

July 1990. The idealized, long-term mean field shown at the upper left was used as the first-guess field for the preliminary map (upper right). The map shown at the bottom left was produced by averaging 31 of the daily preliminary maps, centered on the date shown. In turn, this averaged field was used as the first-guess field for producing the final map shown at the bottom right. Overall, the features of the preliminary and final maps are quite similar, indicating that the mapping procedures are robust. However, careful examination reveals subtle differences between the two. The final map has sharper gradients through the thermocline, and the structure in the slope region is better defined. As discussed in the next section, these slight changes were sufficient to more accurately define the geostrophic velocities.

b. Assessing the accuracy of the Z_{12}^* maps

The quality of the final mapped Z_{12}^* fields is examined in this section. The maps are checked for internal consistency by comparing them with the actual observations. Additionally, the maps are compared with independent measurements of the thermocline depths. Finally, the velocities calculated by differentiating the maps of geostrophic streamfunction determined from Z_{12}^* are compared with observed currents.

1) INTERNAL CONSISTENCY

To compare the Z_{12}^* maps with the actual observations, the mapped thermocline depth at each instrument location was determined by bilinearly interpolating the gridded fields. The differences between the mapped and observed values were calculated for the full deployment period, and subsequently the average differences and standard deviations were determined. For the preliminary maps shown in Fig. 6, the mean offsets were typically ± 5 m, ranging from -13 m at site F2 to $+19$ m at I1. The associated standard deviations ranged from 10 to 16 m. Additionally, there was a noticeable pattern to the offsets; the analyzed values in the northern part of the mapping region were consistently deeper than the observations, while those in the southern regions were shallower. For the final maps, produced using the iterative scheme the offsets were in general less than ± 2 m and, in particular, they were reduced to -3 and $+13$ at sites F2 and I1, respectively. A corresponding reduction was also obtained in the standard deviations, which ranged from 3 to 11 m. Thus, the iterative maps were substantially more consistent with the input data.

2) VERIFICATION AGAINST XBTS

The mapping accuracy was also assessed by comparing independent measurements of the thermocline depth in the study region. For this comparison, XBTs from the IES deployment and recovery cruises as well as XBTs from the Anatomy of Gulf Stream Meanders

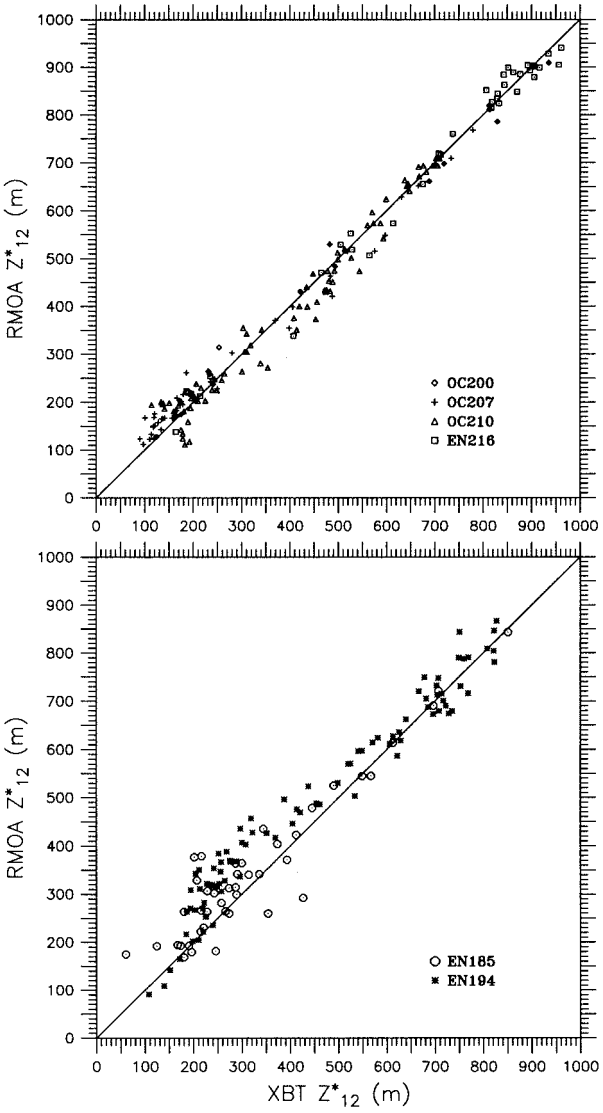

FIG. 8. Comparison of the Z_{12}^* from the objective maps vs the Z_{12}^* from XBTs [determined using Eq. (3) for which Q_T was obtained by integrating the XBT temperatures between 200 and 750 m]. The upper panel shows XBTs from several IES deployment and recovery cruises and the lower panel shows XBTs from the Anatomy experiment. The solid lines indicate the lines of perfect agreement.

experiment (Hummon et al. 1991) were used. For each XBT, Z_{12}^* was calculated from Q_T by integrating the temperature profile, as described previously. XBTs were excluded from this analysis if either 1) their positions occurred in regions where the mapping errors were predicted to be large or 2) they had already been used to determine B_{INT}^* as part of the IES calibrations. The IES mapped fields of Z_{12}^* were linearly interpolated, both spatially and temporally, to compare with the exact position and time of each XBT launch.

In Fig. 8, the Z_{12}^* values obtained from the objective maps are plotted against those of the XBTs. Separate plots are shown for the XBTs from the deployment/

recovery cruises (OC200, OC207, OC210, and EN216) and those from the Anatomy experiment (EN185 and EN194). The rms scatter about the line of perfect agreement is 53 m for Anatomy XBTs and 31 m for the other XBTs. The larger scatter of the Anatomy XBTs rises from a bias of roughly 60 m in the 150–350-m range and a bias of 12 m at deeper levels. Both biases are such that the mapped Z_{12}^* values are deeper than those of the XBTs.

Considerable testing was done to identify the causes of these biases. After processing and timing errors were eliminated as potential causes, the following hypotheses were formed.

Some bias in the 150–350-m depth range is associated with the relatively coarse spacing (55–60 km) of the IESs relative to scales near the north wall of the Gulf Stream. The objective mapping procedure smoothes the Gulf Stream thermal front between the measurement sites. This effect produces a deeper bias near the northern edge of the Gulf Stream, where the thermocline slope changes abruptly from steep to nearly flat [i.e., $Z_{12}^*(y)$ has a large negative curvature]. Half of the Anatomy XBTs were launched in this northern portion of the current (150 m $\leq Z_{12}^* \leq$ 350 m), where the Z_{12}^* maps are biased deeper.

The bias at the deeper levels could arise from navigational offsets. (These cruises preceded the continuous availability of GPS fixes, and so relied upon Loran C.) Because systematic position offsets of 1–2 km have been observed on the same ship when the Northstar internal algorithms were changed for Loran, and the offsets were roughly normal to the coastline and hence roughly normal to the Gulf Stream front, it is not unreasonable to expect that similar offsets might occur between different ships. Such offsets could account for roughly 20 m of the observed differences in Z_{12}^*.

Another source of bias could arise from differences between the portion of the water column measured by the IESs and XBTs. Although the thermocline depth Z_{12}^* is determined as an integral quantity from both types of instruments, the Z_{12}^* from an XBT is based on Q_T in the upper 750 m, whereas the Z_{12}^* from an IES is based on τ measured through the full water column. Variations in temperature structure that occur below the main thermocline will affect the IES Z_{12}^* but not that of the XBT. For example, a 0.3°C change in temperature through a 1000-m range below the thermocline would result in a 1-ms change in travel time, corresponding to a 20-m difference in Z_{12}^*. The IES Z_{12}^* is affected most by the first baroclinic modal structure and is not sensitive to small-scale features in the water column. On the other hand, because the XBT measurement is restricted to the upper 750 m, the Q_T and Z_{12}^* measurements from it can be affected by features of smaller vertical scale. It is estimated that this accounts for about 20 m of the observed scatter in the IES Z_{12}^* versus XBT Z_{12}^* relationship. Since the EN194 XBTs showed the worst bias in Fig. 8 and they all sampled a single meander event, it is conceivable that a higher modal structure might have systematically affected that entire set of measurements. Unfortunately, we know of no way to confirm or refute these hypotheses with the current data.

3) VERIFICATION WITH CURRENT MEASUREMENTS

The final method of assessing the quality of the mapped Z_{12}^* fields was to compare the derived velocity estimates with the observed currents. Just as was done previously for the preliminary set of maps (as described for Fig. 7, second panel), the geostrophic velocity $\mathbf{V}_{\mathrm{OI}}$ was also calculated from the final Z_{12}^* maps. The fourth panel of Fig. 7 shows the time series of $\mathbf{V}_{\mathrm{OI}}$ calculated at site I4.

The similarity of the $\mathbf{V}_{\mathrm{OI}}$ and $\mathbf{V}_{\mathrm{PRE}}$ vectors is not surprising since the preliminary and final Z_{12}^* maps are so similar (Fig. 6). However, careful examination reveals that the magnitudes of the $\mathbf{V}_{\mathrm{OI}}$ vectors are generally larger than those of $\mathbf{V}_{\mathrm{PRE}}$. This increased magnitude improves the agreement with the observed $\mathbf{V}_{\mathrm{CM}}$. The difference vectors (bottom panel) are smaller and no longer show a bias; instead they randomly fluctuate between positive and negative values. Grouping together the data from all 12 current meter sites in the Central Array, the u and v components have rms differences of 13 and 10 cm s^{-1}, respectively (He 1993). He (1993) partially attributes these remaining differences between $\mathbf{V}_{\mathrm{OI}}$ and $\mathbf{V}_{\mathrm{CM}}$ to small-scale circulations that are measured only by the current meters and to errors associated with the OI mapping procedures. However, he finds that the largest differences can be attributed to mesoscale ageostrophic components associated with strong curvature events that are measured by the current meters but are absent in the geostrophic $\mathbf{V}_{\mathrm{OI}}$ velocities.

5. Summary and conclusions

The focus of this paper has been upon several IES data processing steps that have increased the accuracy of the final data products. These procedures include the calibration of individual instruments and the mapping of IES arrays.

A simple method was presented for determining a vertically integrated measure of the thermocline depth from XBTs, which reduces the scatter in the relationship with τ. The conceptual basis for this approach is that the vertical integral of temperature empirically has a clean functional relationship to the travel time measurement (Watts and Rossby 1977). Operationally, XBT profiles are integrated between 200 and 750 m to calculate a quantity Q_T. Subsequently, thermocline depth Z_{12}^* is determined from Q_T using an analytic function. This procedure should be applicable to other ocean regions, but the representative isotherm and the coefficients in Eq. (3) would change to reflect the different regional stratifications.

This approach effectively filters out much of the noise

associated with point measurements. As a result, the scatter of the τ versus Z_{12}^* relationship is 40% smaller than that of the τ versus Z_{12} relationship. The calibration constants are more reliable because nearly all of the outliers are eliminated. The B_{INT}^*, used in the modified (asterisk) versions of Eqs. (1) and (2), has a one standard deviation error of 19 m.

Since seasonal variability is also a source of scatter in the τ versus Z_{12}^* relationship, it is desirable to remove as much of that signal as possible. To determine the seasonal cycle, travel times τ_{200} were calculated from historical XBT profiles by integrating from the surface down to a depth of 200 m. Monthly averages of τ_{200} were determined in cross-stream bins as well as in three along-stream geographic regions. Surprisingly, no significant cross-stream differences were found; only the downstream regions were distinct. The peak-to-peak range of τ_{200} was found to nearly double between Cape Hatteras and 68°W. It is estimated that the average seasonal curves differ by less than 0.3 ms from the seasonal progression during any given year.

Watts et al. (1989) described a method for mapping the thermocline topography measured by IESs onto gridded fields. More recent studies (He 1993; Kim 1994; Lindstrom and Watts 1994) have extended the utility of these maps beyond simple resolution of the Gulf Stream path to diagnosing geostrophic streamfunction and other dynamic quantities related to derivatives of the streamfunction (e.g., velocity and vorticity). However, because those extensions involve differentiating the gridded Z_{12}^* fields, it is crucial for the thermal gradients to be well resolved. This paper shows that the gradients can be sharpened (improving accuracy) by using an iterative mapping scheme. Under this scheme, 31-day-running averages of a preliminary set of maps were used as the first-guess fields for the final set of Z_{12}^* maps. For both steps, the appropriate empirically fitted correlation function was used for optimal interpolation.

Indeed, comparisons with independent measurements confirm that the Z_{12}^* maps can be differentiated with confidence. Specifically, comparisons of actual current observations with the velocities derived from the maps exhibited excellent agreement both in current speed and direction (He 1993). The failure of our earlier mapping attempts to produce good velocities suggests that good results can be obtained only when the input measurements have been interpolated well enough to exhibit the sharp gradients. Comparisons with XBTs from the IES deployment/recovery cruises indicate that Z_{12}^* is mapped with an accuracy of 31 m. However, comparisons with XBTs from the Anatomy experiment cruises conflict with both of these findings, suggesting that the mapping errors are higher for reasons that we have only partly explained. An overall accuracy of 46 m is obtained for the Z_{12}^* maps when the Anatomy XBTs are included.

In this paper, we have demonstrated that IES Z_{12}^* maps of the SYNOP Inlet and Central Arrays are now very consistent with our other datasets. More importantly, however, we can view the fields as accurate daily maps of geostrophic streamfunction. The real payoff in having produced these maps is to be able to use them confidently as ''weather maps'' of the Gulf Stream as has been done by Lindstrom and Watts (1994), Howden (1996), and Lindstrom et al. (1997) with studies of vertical motion and by Kim (1994), who assimilated them into diagnostic models of the Gulf Stream.

Acknowledgments. Initial processing of the SYNOP IESs was performed by Erik Fields. Scott Lindstrom conducted many of the internal consistency tests, and Yuguang He calculated the geostrophic currents from the mapped fields. Tom Rossby and Jules Hummon kindly provided the Anatomy experiment XBTs for additional validation tests. This research was sponsored by the National Science Foundation and the Office of Naval Research.

REFERENCES

Bretherton, F. P., R. E. Davis, and C. B. Fandry, 1976: A technique for objective analysis and design of oceanographic experiments applied to MODE-73. *Deep-Sea Res.,* **23,** 559–582.

Chiswell, S. M., 1994: Using an array of inverted echo sounders to measure dynamic height and geostrophic current in the North Pacific subtropical gyre. *J. Atmos. Oceanic Technol.,* **11,** 1420–1424.

——, D. R. Watts, and M. Wimbush, 1986: Using inverted echo sounders to measure dynamic height in the eastern equatorial Pacific during the 1982–83 El Niño. *Deep-Sea Res.,* **33,** 981–991.

Cronin, M., 1993: Eddy-mean flow interaction in Gulf Stream at 68°W. Ph.D. thesis, University of Rhode Island, 118 pp. [Available from Library, University of Rhode Island, Kingston, RI 02881.]

Fuglister, F. C., and A. D. Voorhis, 1965: A new method of tracking the Gulf Stream. *Limnol. Oceanogr.,* **10,** R115–R124.

Hallock, Z. R., 1987: Regional characteristics for interpreting inverted echo sounder (IES) observations. *J. Atmos. Oceanic Technol.,* **4,** 298–304.

——, 1992: Objective daily maps of thermocline depth for the SYNOP Eastern Array. Naval Oceanographic and Atmospheric Research Laboratory Tech. Note 259, 54 pp. [Available from Naval Research Laboratory, Stennis Space Center, MS 39529-5004.]

He, Y., 1993: Determining the baroclinic geostrophic velocity structure with inverted echo sounders. M.S. thesis, Graduate School of Oceanography, University of Rhode Island, 135 pp. [Available from Library, University of Rhode Island, Kingston, RI 02881.]

Howden, S. D., 1996: Processes associated with steep meander development in the Gulf Stream near 68°W. Ph.D. thesis, University of Rhode Island, 229 pp. [Available from Library, University of Rhode Island, Kingston, RI 02881.]

Hummon, J., T. Rossby, E. Carter, J. Lillibridge, M. Liu, K. Schultz Tokos, S. Anderson-Fontana, and A. Mariano, 1991: The anatomy of Gulf Stream meanders. Vols. 1 and 2. University of Rhode Island, GSO Tech. Rep. 91-4, 488 pp. [Available from Physical Oceanography Dept., Graduate School of Oceanography, Narragansett Bay Campus, University of Rhode Island, Narragansett, RI 02882-1197.]

Iselin, C. O., 1940: Preliminary report on long-period variations in the transport of the Gulf Stream. *Pap. Phys. Oceanogr. Meteor.,* **8,** 1–40.

James, C., M. Wimbush, and H. Ichikawa, 1994: East China Sea Kuroshio 1991–92 data report. University of Rhode Island, GSO Tech. Rep. 94–3, 22 pp. [Available from Physical Oceanography

Dept., Graduate School of Oceanography, Narragansett Bay Campus, University of Rhode Island, Narragansett, RI 02882-1197.]

James, C. E., and M. Wimbush, 1995: Inferring dynamic height variations from acoustic travel time in the Pacific Ocean. *J. Oceanogr.,* **51,** 553–569.

Katz, E. J., 1987: Seasonal response of the sea surface to the wind in the equatorial Atlantic. *J. Geophys. Res.,* **92,** 1885–1893.

Kim, H.-S., 1994: An equivalent-barotropic data-assimilating model of Gulf Stream meanders. Ph.D. thesis, University of Rhode Island, 92 pp. [Available from Library, University of Rhode Island, Kingston, RI 02881.]

——, and D. R. Watts, 1994: An observational streamfunction in the Gulf Stream. *J. Phys. Oceanogr.,* **24,** 2639–2657.

Lee, T., 1994: Variability of the Gulf Stream path observed from satellite infrared images. Ph.D. thesis, University of Rhode Island, 188 pp. [Available from Library, University of Rhode Island, Kingston, RI 02881.]

Li, L., M. Wimbush, D. R. Watts, A. J. Brincko, and T. N. Lee, 1985: Gulf Stream and wind induced current variability on the Georgia continental shelf, winter 1978. *J. Geophys. Res.,* **90,** 3199–3210.

Lindstrom, S. S., and D. R. Watts, 1994: Vertical motion in the Gulf Stream near 68°W. *J. Phys. Oceanogr.,* **24,** 2321–2333.

——, X. Qian, and D. R. Watts, 1997: Vertical motion in the Gulf Stream and its relation to meanders. *J. Geophys. Res.,* **102,** 8485–8503.

Miller, L. L., D. R. Watts, and M. Wimbush, 1985: Oscillations of dynamic topography in the eastern equatorial Pacific. *J. Phys. Oceanogr.,* **15,** 1759–1770.

Rossby, T., 1969: On monitoring depth variations of the main thermocline acoustically. *J. Geophys. Res.,* **74,** 5542–5546.

Shay, T. J., J. M. Bane, D. R. Watts, and K. L. Tracey, 1995: Gulf Stream flow field and events near 68°W. *J. Geophys. Res.,* **100,** 22 565–22 589.

Tracey, K. L., and D. R. Watts, 1986: On Gulf Stream meander characteristics near Cape Hatteras. *J. Geophys. Res.,* **91,** 7587–7602.

——, and ——, 1991: The SYNOP experiment: Thermocline depth maps for the Central Array October 1987 to August 1990. GSO Tech. Rep. 91-5, University of Rhode Island, Narragansett, RI, 193 pp. [Available from Physical Oceanography Dept., Graduate School of Oceanography, Narragansett Bay Campus, University of Rhode Island, Narragansett, RI 02882-1197.]

Trivers, G., and M. Wimbush, 1994: Using acoustic travel time to determine dynamic height variations in the North Atlantic Ocean. *J. Atmos. Oceanic Technol.,* **11,** 1309–1316.

Watts, D. R., and H. T. Rossby, 1977: Measuring dynamic heights with inverted echo sounders: Results from MODE. *J. Phys. Oceanogr.,* **7,** 345–358.

——, and W. E. Johns, 1982: Gulf Stream meanders: Observations on propagation and growth. *J. Geophys. Res.,* **87,** 9467–9476.

——, K. L. Tracey, and A. I. Friedlander, 1989: Producing accurate maps of the Gulf Stream thermal front using objective analysis. *J. Geophys. Res.,* **94,** 8040–8052.

——, ——, J. M. Bane, and T. J. Shay, 1995: Gulf Stream path and thermocline structure near 74°W and 68°W. *J. Geophys. Res.,* **100,** 18 291–18 312.